

# Annihilation range and final-state interaction in $\bar{p}p$ annihilation into $\pi^- \pi^+$

B. El-Bennich,<sup>1,\*</sup> W. M. Kloet,<sup>1</sup> and B. Loiseau<sup>2</sup><sup>1</sup>*Department of Physics and Astronomy, Rutgers University, 136 Frelinghuysen Road, Piscataway, New Jersey 08854, USA*<sup>2</sup>*Laboratoire de Physique Nucléaire et de Hautes Énergies (Groupe Théorie), Université P.& M. Curie, 4 Place Jussieu, F-75252 Paris Cedex 05, France*

(Received 29 January 2003; published 30 July 2003)

The large set of accurate data on differential cross section and analyzing power from the CERN LEAR experiment on  $\bar{p}p \rightarrow \pi^- \pi^+$ , in the range from 360 to 1550 MeV/c, is well reproduced within a distorted wave approximation approach. The initial  $\bar{p}p$  scattering wave functions originate from a recent  $\bar{N}N$  model. The transition operator is obtained from a combination of the  $^3P_0$  and  $^3S_1$  quark-antiquark annihilation mechanisms. A good fit to the data, in particular, the reproduction of the double-dip structure observed in the analyzing powers, requires quark wave functions for proton, antiproton, and pions with radii slightly larger than the respective measured charge radii. This corresponds to an increase in the range of the annihilation mechanisms, and consequently, the amplitudes for total angular momentum  $J=2$  and higher are much larger than in previous approaches. The final-state  $\pi\pi$  wave functions, parametrized in terms of  $\pi\pi$  phase shifts and inelasticities, are also a very important ingredient for the fine tuning of the fit to the observables.

DOI: 10.1103/PhysRevC.68.014003

PACS number(s): 12.39.Jh, 13.75.Cs, 21.30.Fe, 25.43.+t

## I. INTRODUCTION

The very accurate set of data from the LEAR experiment [1] on  $\bar{p}p \rightarrow \pi^- \pi^+$ , measuring the differential cross section and analyzing power from 360 to 1550 MeV/c, is still a challenge for all theoretical models after more than a decade. Large variations are observed in the analyzing power  $A_{0n}$  as a function of angle at all energies, indicating the presence of several partial waves already at low energies. However, recent model calculations [2–7] lead to scattering amplitudes which are strongly dominated by total angular momentum  $J=0$  and  $J=1$ . The reason for this is the choice of a rather short range annihilation mechanism. The short range of the annihilation in the model calculations originates from the dynamics of baryon exchange in Refs. [2–4,7] or from the required overlap of quark and antiquark wave functions for proton and antiproton in Refs. [5,6,8]. On the other hand, the experimental data on differential cross sections as well as those on asymmetries point to a significant  $J=2$ ,  $J=3$ , and even higher  $J$  contributions [9–12].

All above mentioned models, for this reaction, use a distorted wave approximation (DWA). The ingredients for calculating the  $\bar{p}p \rightarrow \pi^- \pi^+$  amplitudes consist of (i) the initial  $\bar{p}p$  scattering wave functions  $\Psi_{\bar{p}p}^-(\mathbf{r})$ , (ii) a transition operator  $O(\mathbf{r}', \mathbf{r})$ , and (iii) the final-state  $\pi\pi$  wave function  $\Psi_{\pi\pi}(\mathbf{r}')$ . The complete scattering amplitude  $T$  itself, constructed in a DWA fashion, is given by

$$T = \int d\mathbf{r}' d\mathbf{r} \Phi_{\pi\pi}(\mathbf{r}') O(\mathbf{r}', \mathbf{r}) \Psi_{\bar{p}p}^-(\mathbf{r}). \quad (1)$$

For example, in Ref. [5] the transition operator  $O(\mathbf{r}', \mathbf{r})$  was obtained from a combination of  $^3P_0$  and  $^3S_1$  quark-antiquark annihilation model,

$$O(\mathbf{r}', \mathbf{r}) = N_0 [V_{3P_0}(\mathbf{r}', \mathbf{r}) + \lambda V_{3S_1}(\mathbf{r}', \mathbf{r})], \quad (2)$$

where the relative strength  $\lambda$  is a complex parameter and  $N_0$  an overall real normalization factor. In the same reference,  $\Psi_{\bar{p}p}^-(\mathbf{r})$  was provided by the 1982 Paris  $\bar{N}N$  potential model [13] and  $\Phi_{\pi\pi}(\mathbf{r}')$  was a simple plane wave. This work did not succeed in reproducing the double-dip structure of the analyzing power and the forward peak in the differential cross section as seen experimentally at, for example, 497 MeV/c. All models referred to above exhibit similar difficulties.

The aim of the present paper is to study possible improvements of the previous models. First of all, mesonic final-state interaction should be considered. The total energy of the  $\bar{p}p \rightarrow 2\pi$  reaction for the studied dataset is in the 2 GeV range. In this energy region, the  $\pi\pi$  interaction is characterized by several resonances [14]. In Refs. [4,6], the role of  $\pi\pi$  final-state interactions was studied. In Ref. [4], some improvement was obtained using a  $\pi\pi$  model reproducing the real part of the  $\pi\pi$  phase shifts with inelasticity parameters in all  $J \neq 0$  partial waves remaining close to 1. In Ref. [6], which explores the  $^3P_0$  part of the quark-antiquark dynamics in the transition operator, the final-state interaction affects mainly observables in the backward region. In both approaches, the double-dip structure observed in the experimental data of the analyzing power remains elusive and further study is still needed. Final-state interactions of two mesons in  $\bar{N}N$  annihilation have also been studied, at quark level, within an extension of the quark rearrangement model [8]. Results were reported for the branching ratios of decays into various two-meson channels. Unfortunately, there are no predictions from this work for differential cross sections or analyzing powers.

Within the approach of Ref. [5], we will study the effect of final-state interactions guided by the  $\pi\pi$  coupled channel model of Ref. [15]. Second, we will study predictions following modification of the annihilation operator  $O(\mathbf{r}', \mathbf{r})$ . As

\*Electronic address: bennich@physics.rutgers.edu

remarked above, this operator has a rather short range in all the present models. The reason for the short range of  $O(\mathbf{r}', \mathbf{r})$  in the quark-antiquark annihilation model, is that the antiproton and proton have a relatively small radius since their quark wave functions describe only the  $qqq$  and  $\bar{q}\bar{q}\bar{q}$  core ignoring the  $\bar{q}q$  cloud. It could be a cause of discrepancy between theory and experiment. In Ref. [5], it has already been noticed that an increase of the annihilation range improves substantially the theoretical description of the data.

In the present work it is shown that the  $\pi\pi$  final-state interaction is a very significant tool for the fine tuning of the fit to the observables. Furthermore, the parameters that determine the sizes of protons and pions are also crucial. An increase of both proton and pion sizes, in closer agreement with their measured radii, allows for a much better fit to the experimental cross sections and analyzing powers. The expressions of the observables in terms of the basic amplitudes together with the DWA ingredients are briefly recalled in Sec. II. The description of the final-state interaction is performed in Sec. III. The modifications of the range of the annihilation mechanisms are studied in Sec. IV. Sec. V presents the final results and the conclusions are summarized in Sec. VI.

## II. OBSERVABLES AND DWA INGREDIENTS

The reaction  $\bar{p}p \rightarrow \pi^- \pi^+$  can be fully described in the helicity formalism by two independent helicity amplitudes  $F_{++}(\theta)$  and  $F_{+-}(\theta)$ . The angle  $\theta$  is the c.m. angle between the outgoing  $\pi^-$  and the incoming  $\bar{p}$ . There are four possible observables [16]

$$\frac{d\sigma}{d\Omega} = \frac{1}{2}(|F_{++}|^2 + |F_{+-}|^2), \quad (3)$$

$$A_{0n} \frac{d\sigma}{d\Omega} = \text{Im}(F_{++}F_{+-}^*), \quad (4)$$

$$A_{\ell s} \frac{d\sigma}{d\Omega} = \text{Re}(F_{++}F_{+-}^*), \quad (5)$$

$$A_{ss} \frac{d\sigma}{d\Omega} = \frac{1}{2}(|F_{++}|^2 - |F_{+-}|^2). \quad (6)$$

So far, only  $d\sigma/d\Omega$  and  $A_{0n}$  have been accurately measured at LEAR [1]. For completeness, we recall here the partial-wave expansion of the helicity amplitudes [16] as

$$F_{++}(\theta) = \frac{1}{p} \sum_J \sqrt{(2J+1)/2} \times [\sqrt{J}f_{J-1}^J - \sqrt{J+1}f_{J+1}^J] P_J(\cos \theta), \quad (7)$$

and

$$F_{+-}(\theta) = \frac{1}{p} \sum_J \sqrt{(2J+1)/2} \times \left[ \sqrt{\frac{1}{J}} f_{J-1}^J + \sqrt{\frac{1}{J+1}} f_{J+1}^J \right] P_J'(\cos \theta). \quad (8)$$

The indices  $J$  and  $L=J\pm 1$  are the total and orbital angular momentum of the  $\bar{p}p$  system, respectively.  $P_J(\cos \theta)$  and  $P_J'(\cos \theta)$  denote a Legendre polynomial and its derivative. The angular momentum of the  $\pi\pi$  system is  $\ell_{\pi\pi} \equiv J$ . Because of parity conservation there are no  $L=J$  amplitudes in the above expansion. The total isospin is  $I=0$  for even  $J$  and  $I=1$  for odd  $J$ . In Eqs. (7) and (8),  $p$  is the magnitude of the antiproton center-of-mass (c.m.) momentum.

The partial-wave amplitudes  $f_L^J$  for  $L=J\pm 1$  are calculated following the DWA method of Eq. (1). One ingredient is the initial coupled spin-triplet  $\Psi_{\bar{p}p}(\mathbf{r})$  wave function in configuration space as obtained in Ref. [17]. The operator  $O(\mathbf{r}, \mathbf{r}')$  is constructed from the quark model description of protons and pions combined with the  ${}^3P_0$  and  ${}^3S_1$  quark-antiquark annihilation and rearrangement mechanism [5]. The last ingredient is the  $\pi\pi$  scattering wave function  $\Phi_{\pi\pi}(\mathbf{r}')$ , which in this paper will be built according to a study of a realistic  $\pi\pi$  scattering model [15], while also comparisons will be made for a simple plane wave  $\pi\pi$  final state. Subsequently, one obtains the differential cross section  $d\sigma/d\Omega$  and the analyzing power  $A_{0n}$  or the left-right asymmetry for the proton target polarized normal to the scattering plane.

## III. FINAL-STATE INTERACTION

First, we assume no interaction between the final pions and describe the  $\pi\pi$  scattering wave function  $\Phi_{\pi\pi}(\mathbf{r}')$  as a plane wave. In this case, the overall normalization of  $d\sigma/d\Omega$  and the relative strength  $\lambda$  between  ${}^3P_0$  and  ${}^3S_1$  annihilation mechanism are parameters to be determined through  $\chi^2$  minimization. Out of the twenty energies where polarization data are available [1], we chose a representative set of five energies,  $T_{\text{lab}} = 66.7, 123.5, 219.9, 499.2,$  and  $803.1$  MeV, corresponding to antiproton momenta of, respectively,  $p_{\text{lab}} = 360, 497, 679, 1089,$  and  $1467$  MeV/c.  $T_{\text{lab}}$  is the laboratory kinetic energy of the antiproton beam. At  $123.5$  MeV ( $p_{\text{lab}} = 497$  MeV/c) and  $219.9$  MeV ( $p_{\text{lab}} = 679$  MeV/c), we do reproduce the results of Ref. [5] using their parameters. Results for the set of five energies are shown in Figs. 1–5 as short-dashed curves. The overall fits are poor with the exception of the analyzing power  $A_{0n}$  at  $803.1$  MeV ( $p_{\text{lab}} = 1467$  MeV/c). The double-dip structure of  $A_{0n}$  is not reproduced at the three lowest energies of the set considered here, which can be attributed to the very small values of the  $J \geq 2$  amplitudes predicted by this model. A lack of substantial  $J \geq 2$  amplitudes is also evident in the predictions for  $d\sigma/d\Omega$  at all energies. The forward peak is poorly reproduced. The backward peak, prominent in the data at  $T_{\text{lab}} = 499.2$  MeV, is also missing in this simplified model. Similar findings were obtained previously at  $T_{\text{lab}} = 123.5$  and  $219.9$  MeV by Ref. [5]. As shown in the analysis of Ref. [11], we recall that large  $J \geq 2$  amplitudes are

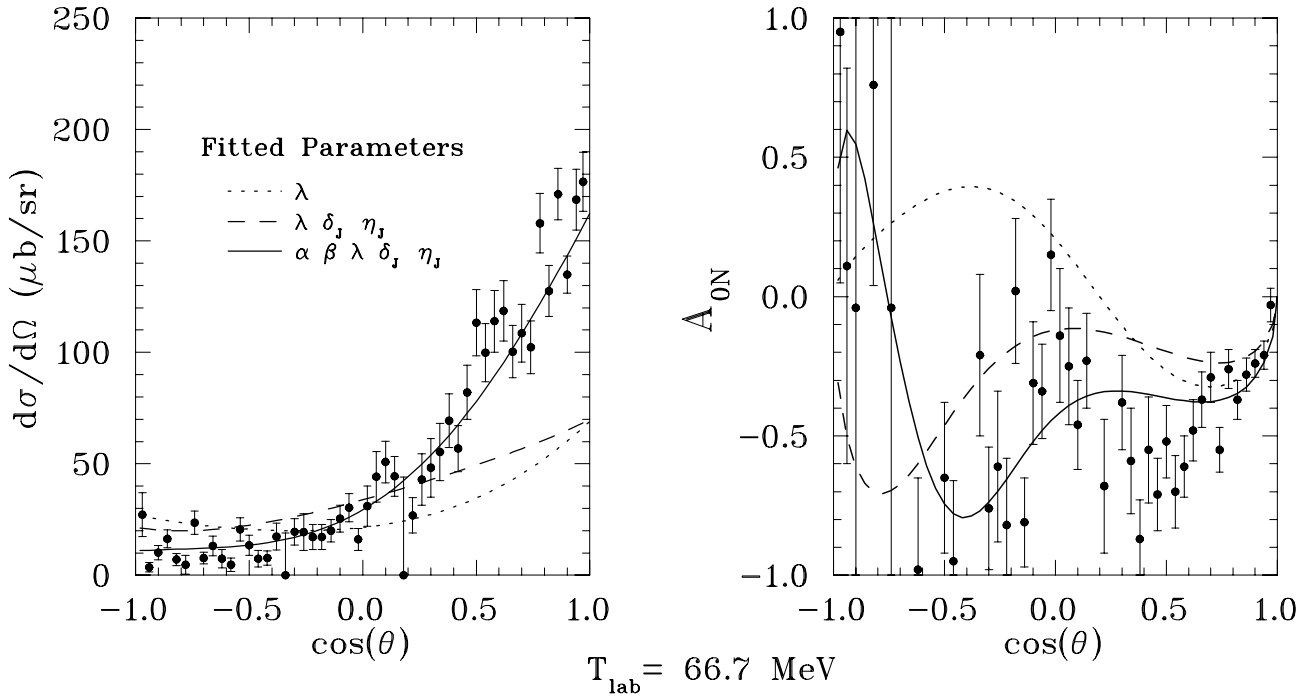


FIG. 1. Differential cross section and analyzing power of the reaction  $\bar{p}p \rightarrow \pi^- \pi^+$  at  $T_{\text{lab}} = 66.7 \text{ MeV}$  ( $p_{\text{lab}} = 360 \text{ MeV}/c$ ). The experimental data are from Hasan *et al.* [1]. The different curves are described in the text.

needed to explain the angular dependence of  $A_{0n}$  and  $d\sigma/d\Omega$ .

One possibility to enhance the amplitudes of higher  $J$  values could be to introduce  $\pi\pi$  final-state interaction. The elastic  $\pi\pi \rightarrow \pi\pi$  amplitude is known from threshold up to

the total relativistic  $\pi\pi$  energy  $\sqrt{s} = 1800 \text{ MeV}$ , mainly from analysis of the  $\pi N \rightarrow \pi\pi N$  reaction. The extracted  $\pi\pi \rightarrow \pi\pi$  amplitudes can be parametrized in terms of phase shifts  $\delta_J$  and inelasticities  $\eta_J$ , where  $J=0, 1, 2,$  and  $3$  [18]. In Ref. [15], a coupled channel model of  $\pi\pi$ ,  $\bar{K}K$ , and  $\rho\rho$

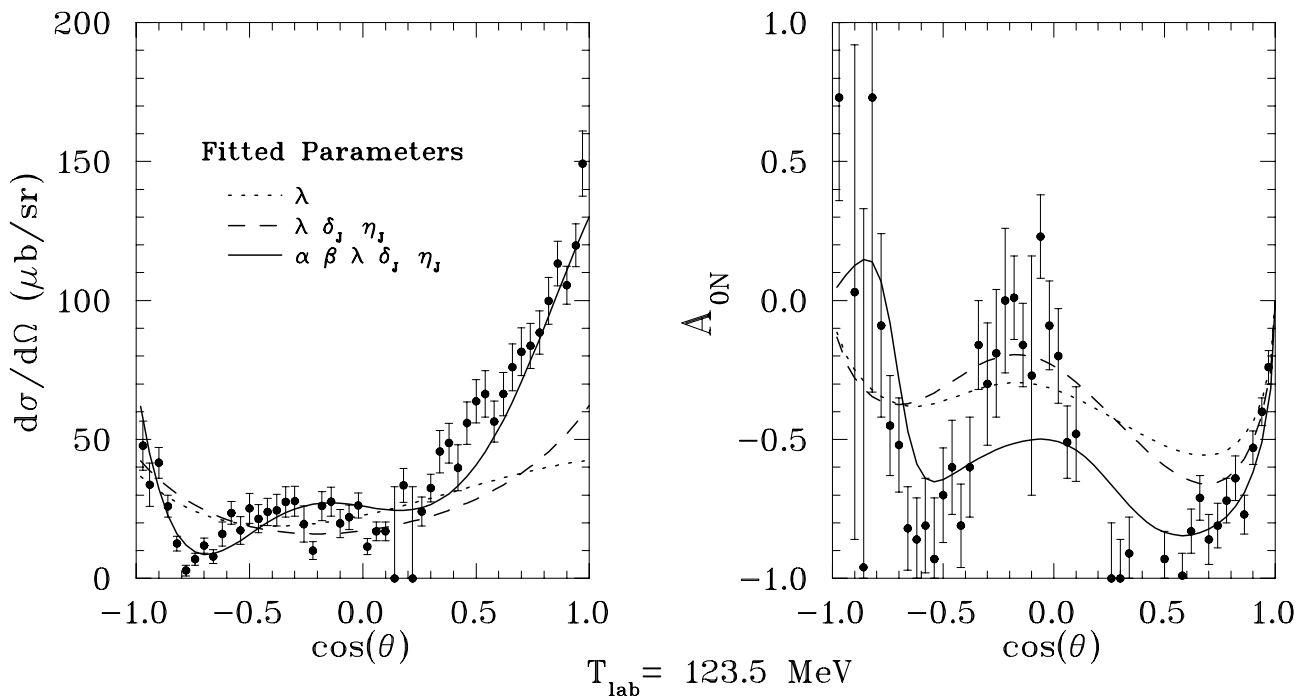


FIG. 2. Same as in Fig. 1, but for  $T_{\text{lab}} = 123.5 \text{ MeV}$  ( $p_{\text{lab}} = 497 \text{ MeV}/c$ ).

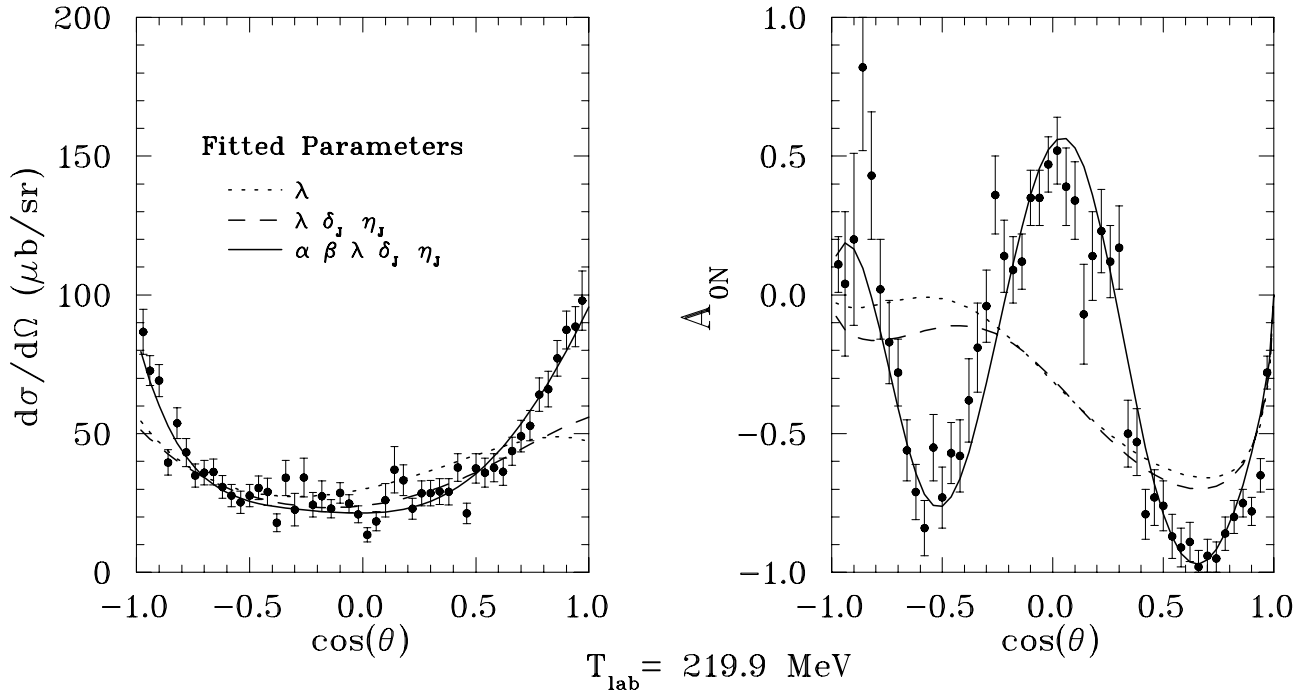


FIG. 3. Same as in Fig. 1, but for  $T_{\text{lab}}=219.9 \text{ MeV}$  ( $p_{\text{lab}}=679 \text{ MeV}/c$ ).

was proposed to reproduce these phase parameters  $\delta_j$  and  $\eta_j$  for  $J=0, 1, 2$ , and  $3$ . The  $\Phi_{\pi\pi}(\mathbf{r}')$  wave functions required for the final-state interaction of  $\bar{p}p \rightarrow \pi\pi$ , can be constructed from this coupled channel model in a straightforward manner. However, since the needed energy range in  $\bar{p}p \rightarrow \pi\pi$  is from  $\sqrt{s}=1910$  to  $2272 \text{ MeV}$ , one has to rely on extrapolation of the coupled channel model results beyond  $\sqrt{s}$

$=1800 \text{ MeV}$ . Calculations with the corresponding  $\Phi_{\pi\pi}(\mathbf{r}')$  show that the observables are very sensitive to the  $\pi\pi$  final-state interaction. Nevertheless, the  $\pi\pi$  scattering amplitude from the extrapolated coupled channel  $\pi\pi$  model still does not improve the predictions of  $\bar{p}p \rightarrow \pi\pi$  obtained previously with just  $\pi\pi$  plane waves. But in this study, we did find that the off-shell part of  $\Phi_{\pi\pi}(\mathbf{r}')$  does play a very minor role. In

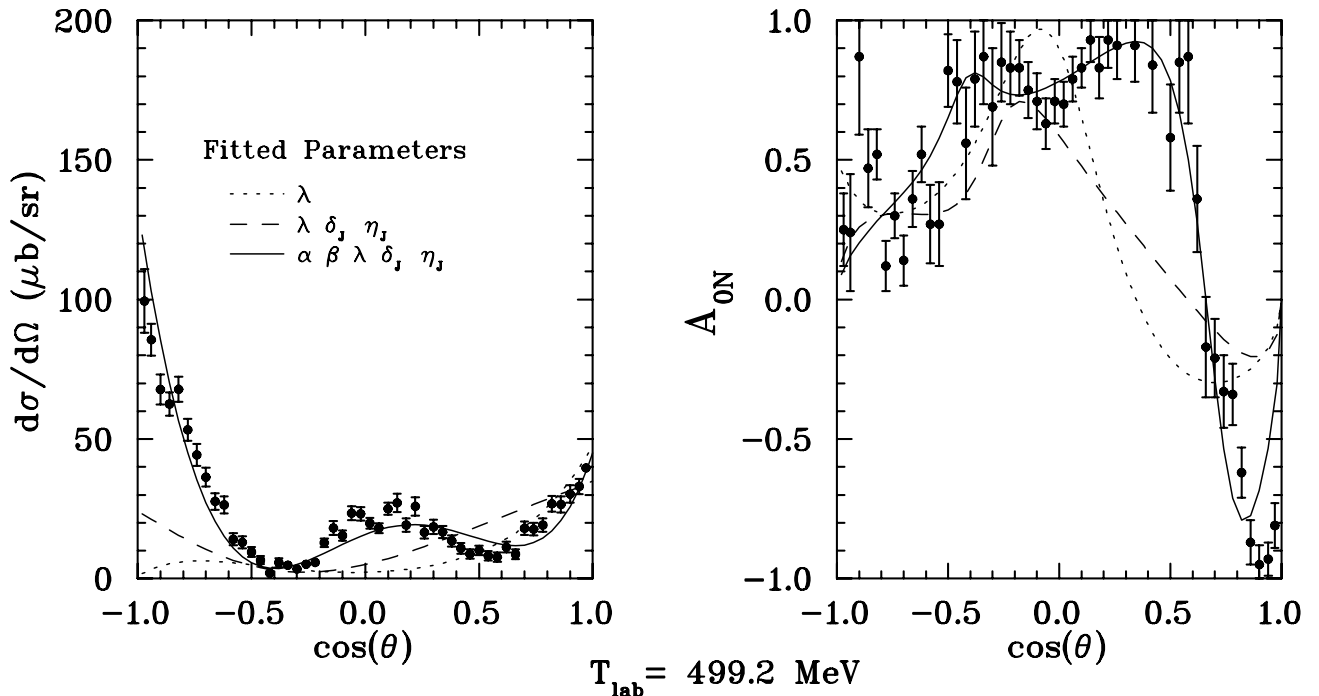


FIG. 4. Same as in Fig. 1, but for  $T_{\text{lab}}=499.2 \text{ MeV}$  ( $p_{\text{lab}}=1089 \text{ MeV}/c$ ).

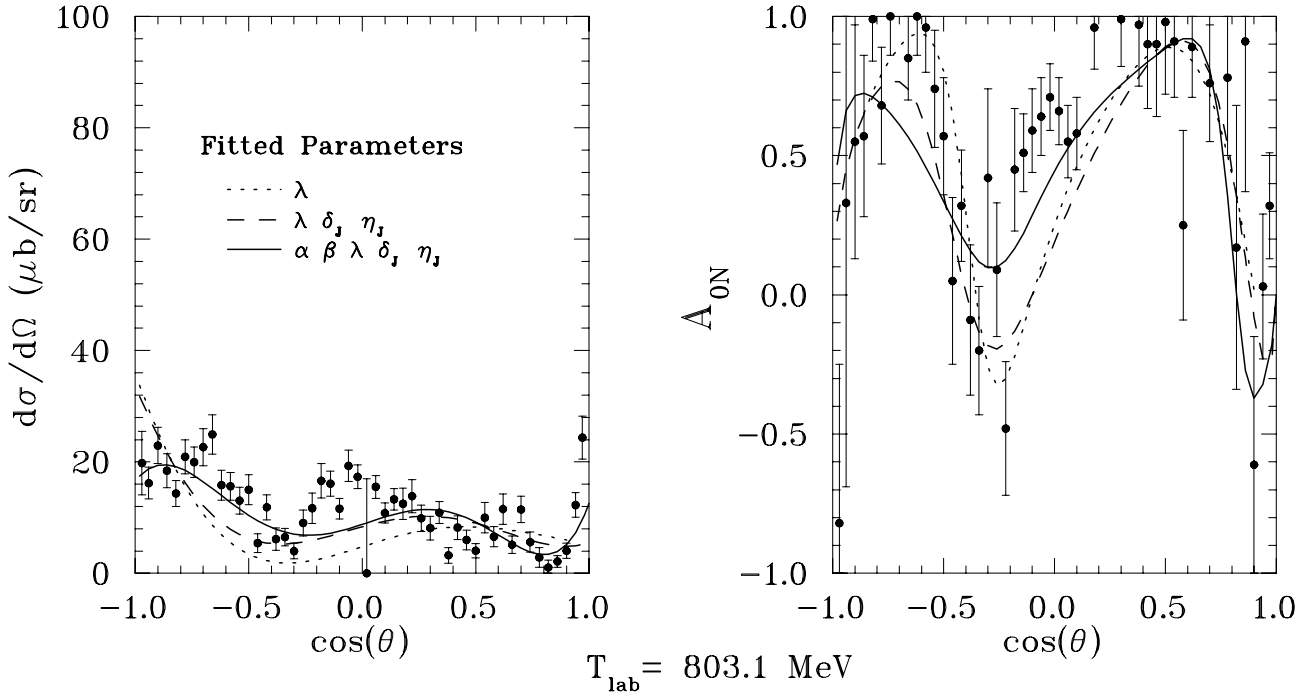


FIG. 5. Same as in Fig. 1, but for  $T_{\text{lab}} = 803.1$  MeV ( $p_{\text{lab}} = 1467$  MeV/c).

particular, it was observed that the same predictions of observables  $d\sigma/d\Omega$  and  $A_{0n}$  can be obtained using only the asymptotic part of the  $\pi\pi$  wave functions. We then exploit this fact by asserting for the remainder of this paper that in  $\bar{p}p \rightarrow \pi\pi$  the unknown  $\pi\pi$  final-state scattering can be fully described by the asymptotic  $\pi\pi$  wave functions parametrized by the  $\pi\pi$  phases  $\delta_J$  and inelasticities  $\eta_J$ .

We then avoid the problem of extrapolation to high  $\sqrt{s}$  by including these new parameters  $\delta_J$  and  $\eta_J$  in the minimization process to obtain realistic fits to  $d\sigma/d\Omega$  and  $A_{0n}$ . Results of this second fitting procedure are shown as the long-dashed curves in Figs. 1–5. Switching on the final-state  $\pi\pi$  interaction improves the fit of  $A_{0n}$  by readjusting the strength of the helicity amplitudes of different  $J$ . This leads to the prediction of a double-dip structure in  $A_{0n}$  at lower energies. This feature is a crucial requirement of the data and shows the need for incorporating the final-state interaction of the pions. However, the predictions for  $d\sigma/d\Omega$  show only a modest improvement over the model without final-state interaction, and the question arises whether there is additional freedom within the model to ameliorate the present fit. So far, the only variable parameter in the annihilation operator is the relative strength  $\lambda$ , unless one allows variations of the range of the annihilation mechanism controlled by the parameters  $\alpha$  and  $\beta$  [5]. In the following section, we will investigate the effects of variations in  $\alpha$  and  $\beta$ .

#### IV. MODIFICATION OF THE ANNIHILATION RANGE

In order to derive the annihilation operator  $O(\mathbf{r}', \mathbf{r})$  (2), one can describe the proton, antiproton, and pions in terms of quarks and antiquarks with the use of Gaussian wave functions [5]. This amounts to approximate quark confine-

ment by solving the Dirac equation with either a scalar or a vector harmonic oscillator potential. The proton (antiproton) intrinsic wave function for the annihilation mechanism is given as

$$\psi_N(\mathbf{r}_1, \mathbf{r}_2, \mathbf{r}_3) = N_N \exp\left[-\frac{\alpha}{2} \sum_{i=1}^3 (\mathbf{r}_i - \mathbf{r}_N)^2\right] \times \chi_N(\text{spin, isospin, color}), \quad (9)$$

where  $\mathbf{r}_i$  are the quark (antiquark) coordinates and  $\mathbf{r}_N$  the nucleon (antinucleon) coordinate. An  $S$ -wave meson intrinsic wave function is given by

$$\phi_M(\mathbf{r}_1, \mathbf{r}_4) = N_M \exp\left[-\frac{\beta}{2} \sum_{i=1,4} (\mathbf{r}_i - \mathbf{r}_M)^2\right] \times \chi_M(\text{spin, isospin, color}). \quad (10)$$

Here  $\mathbf{r}_1$  and  $\mathbf{r}_4$  are the quark and antiquark coordinates, respectively. The coordinate of the meson is  $\mathbf{r}_M$ .

Typical parameter values used before are  $\alpha = 2.80 \text{ fm}^{-2}$  and  $\beta = 3.23 \text{ fm}^{-2}$ , which correspond to a proton (antiproton) radius of 0.60 fm and a meson radius of 0.48 fm [19]. This value of  $\alpha$  describes the  $qqq$  ( $\bar{q}\bar{q}\bar{q}$ ) core of the proton (antiproton), while the measured charge radius, which for the proton is about 0.8 fm, includes also the mesonic cloud. Explicit expressions in terms of  $\alpha$  and  $\beta$  for the transition operators  $V_{3P_0}(\mathbf{r}', \mathbf{r})$  and  $V_{3S_1}(\mathbf{r}', \mathbf{r})$  of Eq. (2) can be found in Ref. [5]. However, one can also argue that in modeling the Gaussian wave functions as in Eqs. (9) and (10), values for  $\alpha$  and  $\beta$  simply should be in accordance with the known charge radii of the proton and pion. The measured pion

charge distribution radius [20] is  $\langle r_\pi^2 \rangle^{1/2} = 0.663 \pm 0.006$  fm. For the proton, we find  $\langle r_p^2 \rangle^{1/2} = 0.870 \pm 0.008$  fm in the literature [14]. We are thus left with a certain freedom when it comes to choosing values for  $\alpha$  and  $\beta$ , and we can wonder about the effects on the annihilation mechanism. The values of the parameters  $\alpha$  and  $\beta$  determine effectively the range of the annihilation mechanism. We can increase the size of the proton and the pion from their original values in Ref. [5] by decreasing  $\alpha$  and  $\beta$ . Then the integration over the intrinsic quark coordinates of, for example, the wave functions  $\psi_p(\mathbf{r}_1, \mathbf{r}_2, \mathbf{r}_3)$ ,  $\psi_{\bar{p}}(\mathbf{r}_4, \mathbf{r}_5, \mathbf{r}_6)$ ,  $\phi_{\pi^+}(\mathbf{r}_1, \mathbf{r}_4)$ , and  $\phi_{\pi^-}(\mathbf{r}_2, \mathbf{r}_5)$  will result in a larger quark overlap. The corresponding annihilation operator  $O(\mathbf{r}', \mathbf{r})$  will have a longer range, and therefore, higher partial waves will contribute to the total amplitude  $T$  in Eq. (1) as required by the analyses of the experimental data of Refs. [9–12].

Changes of  $\alpha$  and  $\beta$  can furthermore be linked to relativistic corrections of the pion wave function  $\phi_M(\mathbf{r}_1, \mathbf{r}_4)$ , as the kinetic energy of the outgoing pion is much larger than its rest-mass energy. In practical terms, this means that in the center of mass, where the calculation is performed, the pion wave function should not be described as a sphere anymore. A proper treatment requires a Lorentz boost of the pion intrinsic wave function from its rest frame to the c.m. frame. Thus, one expects a change in the geometry of the Gaussian shape of the pion [21]. This affects the overlap integral (1) which could be mocked by a simultaneous alteration of  $\alpha$  and  $\beta$ . We therefore take  $\alpha$  and  $\beta$  to be variable parameters to the extent that they still satisfy physical conditions.

## V. FINAL FIT

The results of our final fit, which now includes values of the parameters  $\alpha, \beta, \lambda = |\lambda| \exp(i\theta_\lambda), \delta_J, \eta_J$ , and of the overall normalization  $N_0$  are shown as solid curves in Figs. 1–5. The improvement over the previous fits is dramatic but requires both increased sizes of the antiproton, proton, and pions as well as a tuned final-state interaction. The main achievement is the reproduction in the differential cross section  $d\sigma/d\Omega$  of the characteristic forward peaks at lower energies ( $T_{\text{lab}} = 66.7, 123.5, \text{ and } 219.9$  MeV) and backward peaks at higher energies ( $T_{\text{lab}} = 219.9$  and  $499.2$  MeV). This clearly indicates that the increase of the annihilation range now produces much larger amplitudes for  $J=2$  and higher. The predictions for the double-dip structure of the analyzing power  $A_{0n}$  compare much better with the experimental results especially for  $T_{\text{lab}} \geq 219.9$  MeV.

In addition to the double-dip structure of  $A_{0n}$ , the experimental data display another characteristic feature: the asymmetry shifts from predominantly negative values at lower energies toward positive values at higher energies. Our final fit accounts for this pattern. The quark model parameters  $\alpha, \beta, \lambda$ , and the overall norm  $N_0$  resulting from this fit are listed in Table I and the phase shifts  $\delta_J$  and inelasticities  $\eta_J$  of the final-state interaction with their dependence on  $\sqrt{s}$  in Table II. Note that the latter have been readjusted in the final fit and differ from the  $\delta_J$  and  $\eta_J$  obtained in the fit presented in Sec. III. The  $\pi\pi$  phases for  $J=0,1$  are small but for  $J$

TABLE I. Quark model parameters as function of  $T_{\text{lab}}$ .

$T_{\text{lab}}(\text{MeV})$	66.7	123.5	219.9	499.2	803.1
$p_{\text{lab}}(\text{MeV}/c)$	369	497	679	1089	1467
$\alpha$ (fm $^{-2}$ )	1.20	1.19	1.11	1.20	1.20
$\beta$ (fm $^{-2}$ )	1.54	1.51	1.00	1.54	1.54
$ \lambda $	1.200	1.064	0.662	0.545	0.424
$\theta_\lambda$ ( $^\circ$ )	197.10	125.68	166.83	176.32	183.29
$N_0$ ( $10^5$ )	5.251	4.804	5.046	4.222	4.667

$=2,3,4$  they are substantial. The inelasticities  $\eta_J$ , in particular for  $J=2$ , may indicate the presence of resonances in this channel. From Table I, it is also clear that the parameters  $\alpha$  and  $\beta$  are almost constant with energy but have lower values at 219.9 MeV. Nevertheless, in Fig. 6, we show (long-dashed line) that one can obtain a fit of similar quality, keeping the size parameters  $\alpha = 1.09$  fm $^{-2}$  and  $\beta = 1.51$  fm $^{-2}$  close to the values at the other four energies. The relative strength  $\lambda$  exhibits an energy dependence. This dependence shows a smooth decrease of  $|\lambda|$  with increasing  $\sqrt{s}$ , which indicates that the  ${}^3P_0$  mechanism preponderates at higher energies. The phase  $\theta_\lambda$  of  $\lambda$  should be compared with the value  $\theta_\lambda = 180^\circ$  of Ref. [5]. Furthermore, we find that  $\alpha$  decreases by about a factor of 2.3, while  $\beta$  decreases by about a factor of 2.2. In other words, the proton size in this model increases to  $\langle r_p^2 \rangle^{1/2} = 0.91$  fm and the pion radius is now  $\langle r_\pi^2 \rangle^{1/2} = 0.71$  fm, which is within 7% of the values of Refs. [14,20] mentioned in the preceding section.

The dramatic improvement that occurs when the size parameters  $\alpha$  and  $\beta$  take on smaller values, tends to mask the equally important role of the final-state interaction. If the final-state interaction is turned off from the very beginning by fixing the phase parameters  $\delta_J=0$  and  $\eta_J=1$  while  $\alpha, \beta, \lambda$  are allowed to vary,  $\alpha$  and  $\beta$  again decrease significantly, which confirms an increased annihilation range within our model. Nevertheless, the resulting fit without final-state interaction is far from satisfactory and it is only when we include final-state interaction that we recover the fit quality discussed earlier in this section. This is illustrated at  $T_{\text{lab}}$

TABLE II. Phases shifts  $\delta_J$  and inelasticities  $\eta_J$  of the final-state interaction for  $0 \leq J \leq 4$  as function of  $\sqrt{s}$ .

$T_{\text{lab}}(\text{MeV})$	66.7	123.5	219.9	499.2	803.1
$\sqrt{s}$ (MeV)	1910.0	1937.0	1983.0	2111.0	2242.0
$\eta_0$	0.840	0.989	0.937	1.00	1.00
$\delta_0$	-4.57	-4.37	-6.59	-5.24	-0.63
$\eta_1$	0.998	0.995	0.921	0.999	0.914
$\delta_1$	8.05	4.89	-4.14	-3.24	-1.88
$\eta_2$	0.756	0.669	0.760	0.818	0.309
$\delta_2$	35.74	24.49	55.57	37.66	74.95
$\eta_3$	1.00	1.00	0.808	1.00	1.00
$\delta_3$	59.66	41.41	62.45	48.15	-19.59
$\eta_4$	1.00	0.997	0.858	1.00	0.990
$\delta_4$	36.93	-41.29	6.19	-60.70	61.77

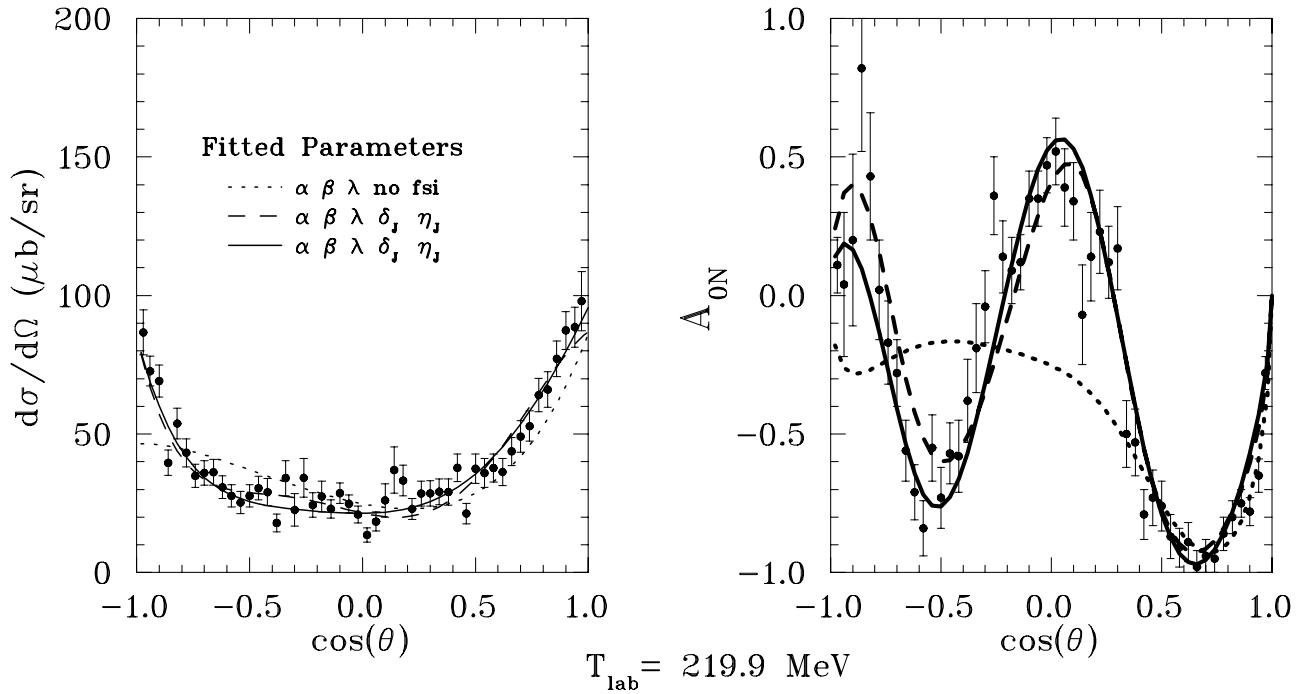


FIG. 6. Various fits for  $T_{\text{lab}}=219.9 \text{ MeV}$  ( $p_{\text{lab}}=679 \text{ MeV}/c$ ). The solid curve is the same as in Fig. 3. The long-dashed curve represents a fit with final-state interaction, where  $\alpha=1.09 \text{ fm}^{-2}$  and  $\beta=1.51 \text{ fm}^{-2}$ . The short-dashed curve is a fit with no final-state interaction, where  $\alpha=1.27 \text{ fm}^{-2}$  and  $\beta=1.53 \text{ fm}^{-2}$ .

$=219.9 \text{ MeV}$  ( $p_{\text{lab}}=679 \text{ MeV}/c$ ) in Fig. 6. The short-dashed curve represents the fit without final-state interaction, and for which  $\alpha=1.27 \text{ fm}^{-2}$  and  $\beta=1.53 \text{ fm}^{-2}$ . This short-dashed curve in Fig. 6 should be compared with the short-dashed curve in Fig. 3, for which  $\alpha=2.80 \text{ fm}^{-2}$  and  $\beta$

$=3.23 \text{ fm}^{-2}$ . The differential cross section has improved significantly in the forward hemisphere. However, the analyzing power is only marginally better. The solid line of Fig. 6 is with inclusion of the final-state interaction. Similar results are obtained at the other energies, which confirms that

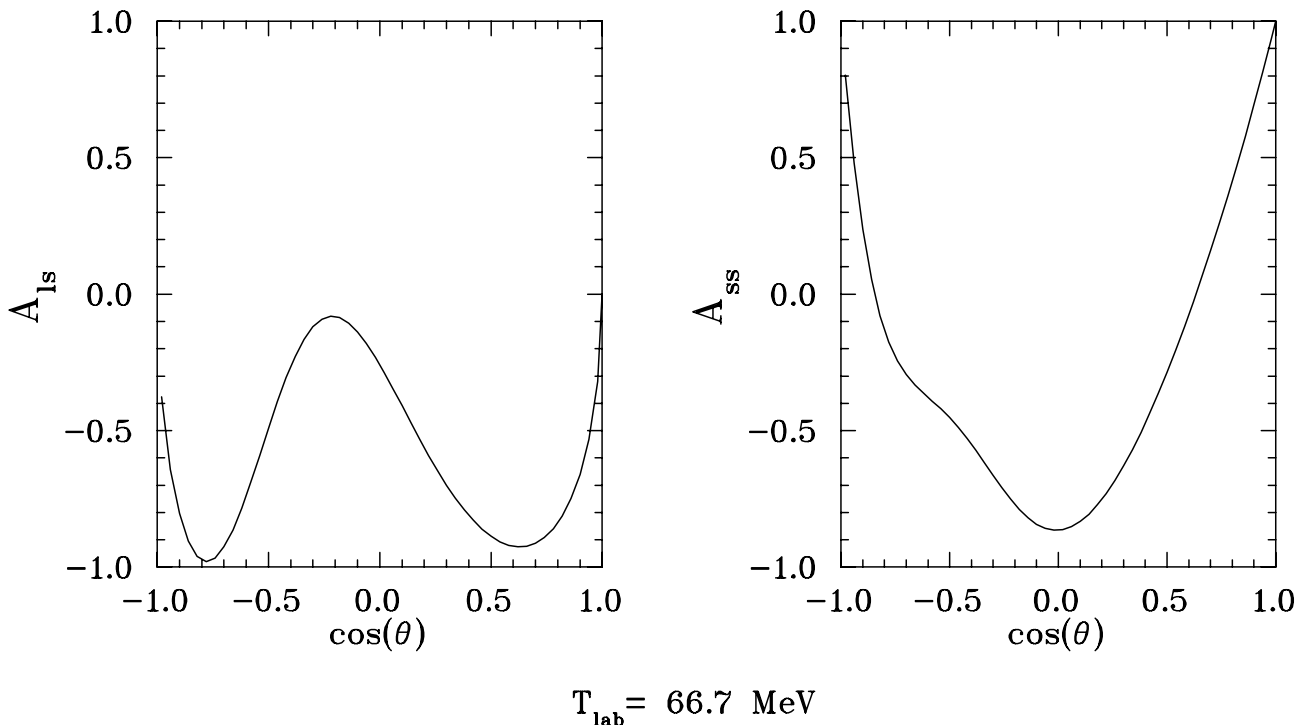
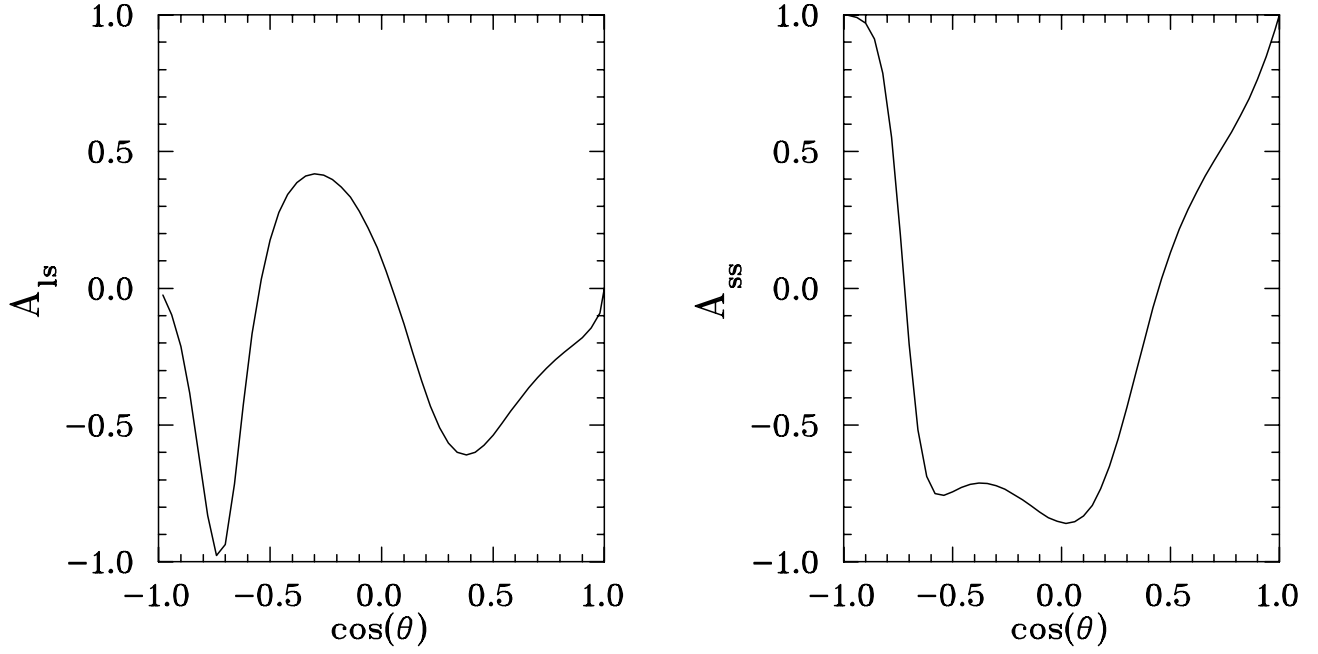


FIG. 7. Predictions at  $T_{\text{lab}}=66.7 \text{ MeV}$  ( $p_{\text{lab}}=360 \text{ MeV}/c$ ) for the observables  $A_{\not{s}}$  and  $A_{ss}$  obtained with the final fit.



$T_{\text{lab}} = 123.5 \text{ MeV}$

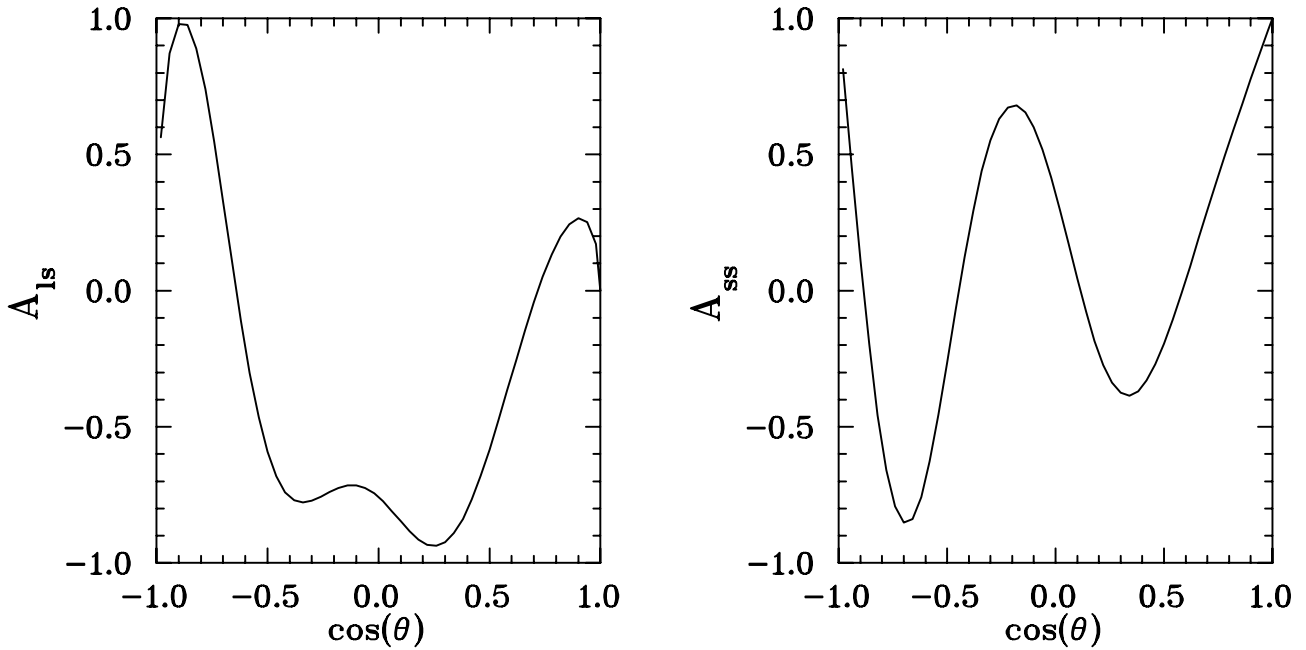
FIG. 8. Same as in Fig. 7, but for  $T_{\text{lab}}=123.5 \text{ MeV}$  ( $p_{\text{lab}}=497 \text{ MeV}/c$ ).

in order to reproduce the LEAR data, both an increased annihilation range as well as interaction in the final  $\pi\pi$  state are necessary.

With the present parameters, we can proceed to compute other spin observables for the  $\bar{p}p \rightarrow \pi^- \pi^+$  reaction. We take the opportunity to present, for each energy considered above,

the predictions for the spin observables  $A_{\ell s}$  and  $A_{ss}$  introduced in Eqs. (5) and (6). We remind the reader that the spin observables are related by

$$A_{0n}^2 + A_{\ell s}^2 + A_{ss}^2 = 1, \tag{11}$$



$T_{\text{lab}} = 219.9 \text{ MeV}$

FIG. 9. Same as in Fig. 7, but for  $T_{\text{lab}}=219.9 \text{ MeV}$  ( $p_{\text{lab}}=679 \text{ MeV}/c$ ).

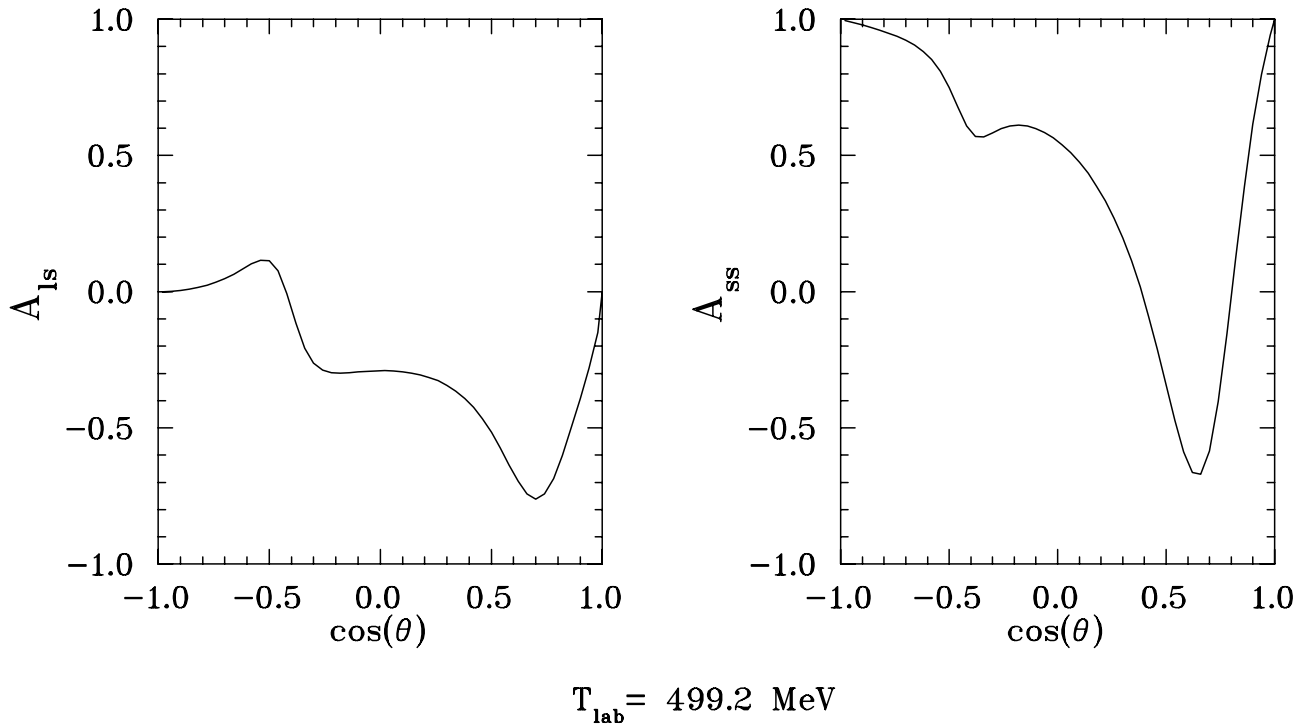


FIG. 10. Same as in Fig. 7, but for  $T_{\text{lab}}=499.2 \text{ MeV}$  ( $p_{\text{lab}}=1089 \text{ MeV}/c$ ).

and that the reaction  $\bar{p}p \rightarrow \pi^- \pi^+$  has only three independent observables within a sign ambiguity, and of course,  $d\sigma/d\Omega$  is chosen as one of them. At each energy, the corresponding parameters of Tables I and II are used. The results are shown in Figs. 7–11. The spin observables  $A_{\ell s}$  and  $A_{ss}$  exhibit again the typical structure with two extrema as a function of

angle, which take often the form of a double dip. There is as yet no data to compare with.

## VI. CONCLUSION

The extensive set of data of differential cross sections  $d\sigma/d\Omega$  and analyzing powers  $A_{0n}$  from the LEAR experi-

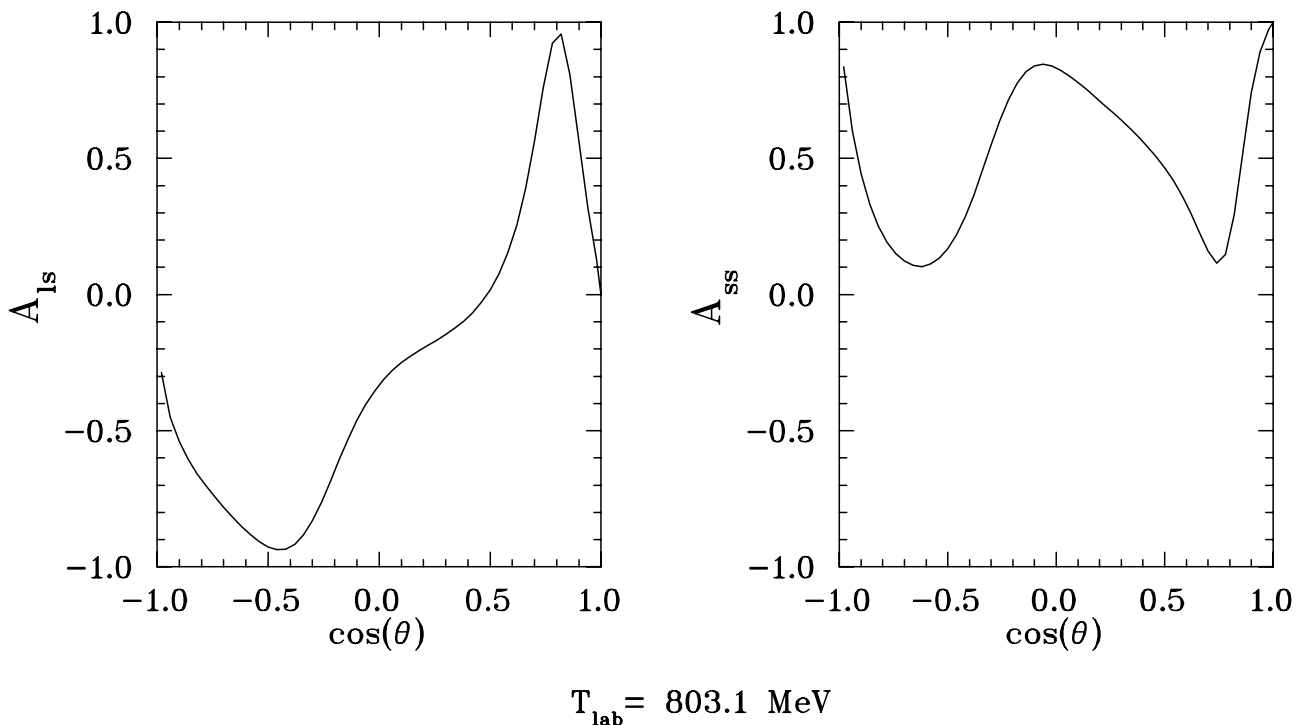


FIG. 11. Same as in Fig. 7, but for  $T_{\text{lab}}=803.1 \text{ MeV}$  ( $p_{\text{lab}}=1467 \text{ MeV}/c$ ).

ment [1] on  $\bar{p}p \rightarrow \pi^- \pi^+$  in the range  $p_{\text{lab}} = 360\text{--}1550$  MeV/ $c$  can be fitted by the combined mechanisms  ${}^3P_0$  and  ${}^3S_1$  of the quark-antiquark annihilation model.

The initial  $\bar{p}p$  relative wave functions were taken from Ref. [17]. It is important to include the final-state  $\pi\pi$  interaction and employ quark wave functions for proton, antiproton, and pions with radii which are slightly larger than the respective measured charge radii. Previously used hadron intrinsic quark wave functions [5] describe only the quark core of the hadrons without the  $\bar{q}q$  cloud, and their parameters therefore correspond to a considerably smaller radius. Increased hadronic radii lead to an increase in the range of the annihilation mechanism, and as a result, amplitudes for  $J=2$  and higher are much larger than before. This feature in the model is essential since the experimental data on  $A_{0n}$  exhibit a double dip, which indicates the presence of substantial amplitudes of  $J=2$  and higher, already at lower mo-

menta  $p_{\text{lab}}$ . The relative strength of the  ${}^3P_0$  and  ${}^3S_1$  mechanisms shows a smooth energy dependence and suggests that the  ${}^3P_0$  mechanism becomes more dominant at the higher energies. It is however noted that the pronounced forward and backward peaks in the cross section require the presence of both  ${}^3P_0$  and  ${}^3S_1$  mechanisms.

#### ACKNOWLEDGMENTS

B.E. and W.M.K. thank the LPNHE and its Groupe Théorie for their warm and stimulating hospitality. B.L. wishes to acknowledge the welcome and support of the Department of Physics and Astronomy of Rutgers University during his visits. Laboratoire de Physique Nucléaire et de Hautes Énergies is Unité de Recherche des Universités Paris 6 et Paris 7 associée au CNRS. This research was supported in part by the U.S. National Science Foundation Grant No. Phy-9722088.

- 
- [1] A. Hasan *et al.*, Nucl. Phys. **B378**, 3 (1992).  
 [2] B. Moussallam, Nucl. Phys. **A407**, 413 (1983); **A429**, 429 (1984).  
 [3] V. Mull, J. Haidenbauer, T. Hippchen, and K. Holinde, Phys. Rev. C **44**, 1337 (1991).  
 [4] V. Mull, K. Holinde, and J. Speth, Phys. Lett. B **275**, 12 (1992).  
 [5] G. Bathas and W.M. Kloet, Phys. Rev. C **47**, 2207 (1993); Phys. Lett. B **301**, 155 (1993).  
 [6] A. Muhm, T. Gutsche, R. Thierauf, Y. Yan, and Amand Faessler, Nucl. Phys. **A598**, 285 (1996).  
 [7] Y. Yan and R. Tegen, Phys. Rev. C **54**, 1441 (1996); Nucl. Phys. **A648**, 89 (1999).  
 [8] A.M. Green and G.Q. Liu, Nucl. Phys. **A486**, 581 (1988).  
 [9] M.N. Oakden and M.R. Pennington, Nucl. Phys. **A574**, 731 (1994).  
 [10] A. Hasan and D.V. Bugg, Phys. Lett. B **334**, 215 (1994).  
 [11] W.M. Kloet and F. Myhrer, Phys. Rev. D **53**, 6120 (1996).  
 [12] B.R. Martin and G.C. Oades, Phys. Rev. C **56**, 1114 (1997); **57**, 3492 (1998).  
 [13] J. Côté, M. Lacombe, B. Loiseau, B. Moussallam, and R. Vinh Mau, Phys. Rev. Lett. **48**, 1319 (1982).  
 [14] Particle Data Group, K. Hagiwara, Phys. Rev. D **66**, 010001 (2002).  
 [15] W.M. Kloet and B. Loiseau, Eur. Phys. J. A **1**, 337 (1998).  
 [16] A.D. Martin and M.R. Pennington, Phys. Lett. **86B**, 93 (1979); A.D. Martin and M.R. Pennington, Nucl. Phys. **B169**, 216 (1980).  
 [17] B. El-Bennich, M. Lacombe, B. Loiseau, and R. Vinh Mau, Phys. Rev. C **59**, 2313 (1999).  
 [18] S. Protopopescu *et al.*, Phys. Rev. D **7**, 1279 (1973); G. Grayer *et al.*, Nucl. Phys. **B75**, 189 (1974); B. Hyams, *et al.*, *ibid.* **B100**, 205 (1975); L. Rosselet *et al.*, Phys. Rev. D **15**, 574 (1977); D.V. Bugg, A.V. Sarantsev, and B.S. Zou, Nucl. Phys. **B471**, 59 (1996); R. Kamiński, L. Leśniak, and K. Rybicki, Acta Phys. Pol. C **B74**, 79 (1997); R. Kamiński, L. Leśniak, and K. Rybicki, Acta Phys. Pol. B **31**, 895 (2000); E865 Collaboration, S. Pislak *et al.*, Phys. Rev. Lett. **87**, 221801 (2001); R. Kamiński, L. Leśniak, and K. Rybicki, Eur. Phys. J. C **4**, 1 (2002).  
 [19] A.M. Green and J.A. Niskanen, Nucl. Phys. **A412**, 448 (1984); **A430**, 605 (1984); Mod. Phys. Lett. A **1**, 441 (1986).  
 [20] S. Amendolia *et al.*, Nucl. Phys. **B277**, 168 (1986).  
 [21] B. El-Bennich and W. M. Kloet (unpublished).